Research Article

Muhammad Nasir, Muhammad Waqas, O. Anwar Bég, D. Baba Basha*, N. Zamri, H. J. Leonard, and Ilyas Khan*

Chemically reactive Maxwell nanoliquid flow by a stretching surface in the frames of Newtonian heating, nonlinear convection and radiative flux: Nanopolymer flow processing simulation

https://doi.org/10.1515/ntrev-2022-0078
received January 3, 2022; accepted February 16, 2022

Abstract: The effects of a chemical reaction and radiative heat flux in a nonlinear mixed thermo-solutal convection flow of a viscoelastic nanoliquid from a stretchable surface are investigated theoretically. Newtonian heating is also considered. The upper-convected Maxwell (UCM) model is deployed to represent the non-Newtonian characteristics. The model also includes the influence of thermal radiation that is simulated *via* an algebraic flux model. Buongiorno's two-component nanofluid model is implemented for thermophoretic and Brownian motion effects. Convective thermal and solutal boundary conditions are utilized to provide a more comprehensive evaluation of temperature and concentration distributions. Dimensionless equations are used to create the flow model by utilizing the appropriate parameters. The computed models are presented through a convergent homotopic analysis method (HAM) approach with the help of Mathematica-12 symbolic software. Authentication of HAM solutions with special cases from the literature is presented. The impact of various thermophysical, nanoscale and rheological parameters on transport characteristics is visualized graphically and interpreted in detail. Temperatures are strongly enhanced with Brownian motion and thermophoresis parameters. Velocity is boosted with the increment in the Deborah viscoelastic number and mixed convection parameter, and the hydrodynamic boundary layer thickness is reduced. A stronger generative chemical reaction enhances concentration magnitudes, whereas an increment in the destructive chemical reaction reduces them and also depletes the concentration boundary layer thickness. Temperature and concentration are also strongly modified by the conjugate thermal and solutal parameters. Greater radiative flux also enhances the thermal boundary layer thickness. Increasing the Schmidt number and the Brownian motion parameter diminish the concentration values, whereas they elevate the Sherwood number magnitudes, *i.e.* enhance the nanoparticle mass transfer rate to the wall.

Keywords: thermal radiation, stretching surface, Maxwell nanoliquid, chemical reaction, homotopy analysis method, Deborah number, nanopolymeric manufacturing, thermo-solutal transport, Sherwood number

*** Corresponding author: D. Baba Basha,** Department of Information Sciences, College of Computer and Information Sciences, Majmaah University, Al-Majmaah, 11952, Saudi Arabia, e-mail: b.dudekula@mu.edu.sa
*** Corresponding author: Ilyas Khan,** Department of Mathematics, College of Science Al-Zulfi, Majmaah University, Al-Majmaah 11952, Saudi Arabia, e-mail: i.said@mu.edu.sa
Muhammad Nasir, N. Zamri: Faculty of Informatics and Computing, University Sultan Zainal Abidin (Kampus Gong Badak), Kuala Terengganu, Terengganu 21300, Malaysia, e-mail: si3775@putra.unisza.edu.my
Muhammad Waqas: NUTECH School of Applied Science and Humanities, National University of Technology, Islamabad 44000, Pakistan, e-mail: mw_qau88@yahoo.com
O. Anwar Bég: Multi-Physical Engineering Sciences Group, Mechanical Engineering, Salford University, School of Science, Engineering and Environment (SEE), Manchester, M54WT, United Kingdom, e-mail: O.A.Beg@salford.ac.uk
H. J. Leonard: Multi-Physical Engineering Sciences Group, Mechanical Engineering, Salford University, School of Science, Engineering and Environment (SEE), Manchester, M54WT, United Kingdom, e-mail: H.Leonard@salford.ac.uk

1 Introduction

In recent years, non-Newtonian (rheological) fluid transport phenomena have received a great deal of interest from scientists and researchers due to diverse applications in industrial applications [1]. Many biotechnological and process mechanical engineering fluent media are non-Newtonian and common examples include gels,

adhesives, polymers, foodstuffs, foams, slurries, emulsions, paints, blood, tribological suspensions, gypsum paste, glass melts, petroleum fluids, *etc.* Polymers in particular exhibit many complex rheological characteristics. For example, at a constant molecular weight, the amount of energy required to process a polymer is directly related to the shear rate dependence of the polymer viscosity. Some important manufacturing processes involving polymers are viscoelastic abrasive flow machining [2], micromixing [3], squeezing flows [4] and stretching and retraction dynamics of films/sheets [5]. Non-Newtonian materials have unique properties that cannot be explained by a single constitutive model. A number of constitutive equation models have therefore been constructed by researchers to simulate the behaviour of non-Newtonian liquids. These include the Oldroyd-B, Giesekus (Gsk), and Phan Thien-Tanner (PTT) models, which are viscoelastic models, the Bingham viscoplastic model, and the Ostwald–de Waele power-law model for pseudoplastic or dilatant fluids. In parallel with the rheometric experimental studies, considerable activity has been motivated in mathematical and computational modelling of non-Newtonian flows, often with heat and mass transfer. These studies feature highly nonlinear and coupled boundary value problems that generally require sophisticated analytical techniques, *e.g.* homotopy methods, variational iteration methods, Adomian decomposition, *etc.* Often, numerical methods are also used that may include finite element, finite difference and spectral methods. Many excellent studies of non-Newtonian flows from a stretching surface have been communicated since this regime is fundamental to polymeric flow processing systems. Huang *et al.* [6] utilized the Chebyshev finite difference method (ChFD) to simulate the significance of thermoviscosity (viscosity depending on the temperature) on the unsteady flow and heat transfer in a power-law liquid film from a stretching sheet. They showed that thermoviscosity strongly enhances the film thickness and the local heat-transfer rate (Nusselt number). Anwar Bég *et al.* [7] implemented an electrothermal network solver (PSPICE) to investigate the unsteady buoyancy-driven convection boundary-layer flow of a magnetic Walters-B viscoelastic polymer from a stretching surface in porous media, noting that velocity is increased with viscoelastic parameter while it is suppressed with the magnetic field. They also noted that an increasing thermal Grashof number inhibits the flow and an increasing suction at the sheet reduces the temperatures. An alternative rheological model is the upper-convected Maxwell viscoelastic model, which also has excellent accuracy for simulating certain polymer flows. This model is an example of a rate-type model in which the relaxation and retardation times are defined. It is particularly valuable for small molecular significance polymers since it allows for a reasonable estimation of stress relaxation and retardation. The viscosity of long-branched polymers is more shear rate-dependent than is the viscosity of linear polymers, and the long-chain branching affects the elasticity of the polymer melts, which is seen in the normal stress difference and the storage modulus [1]. Shahid *et al.* [8] investigated the non-Fourier heat and mass transfer in magnetized upper-convected Maxwell fluid flow from a permeable stretching sheet. They utilized the successive Taylor series linearization method (STSLM) with Gauss–Lobatto collocation and Chebyshev interpolating polynomials and noted a strong modification in the Nusselt number, Sherwood number and skin friction with a change in the viscoelastic parameter.

An important development in the 21st-century engineering sciences has been the deployment of nanomaterials. Engineered at the nanoscale, such materials include graphene, matrix composites with embedded carbon nanotubes (CNTs) and nanopolymers. Nanopolymers are an example of nanofluids in which the base fluid is modified with the dispersal of nanosized particles. The nanoparticles may be metallic (*e.g.* copper, zinc, silver, *etc.*) or carbon-based (silicon, diamond, *etc.*), and the resulting nanofluid is termed unitary. Combinations of nanoparticles may also be used to produce hybrid nanofluids. Base fluids may be aqueous, oil, polymeric, *etc.* The inclusion of metallic nanoparticles, in particular, has been shown to achieve exceptional enhancement in thermal properties of the resulting solid–liquid composite material, *i.e.* colloidal suspension (nanofluid) [9]. Viscosity is also substantially modified in nanofluids as reviewed lucidly by Ilyas *et al.* [10]. Theoretical studies of nanofluid flows have also mobilized considerable interest and involve a combination of fluid dynamics, thermal convection and thermal conduction among other aspects. Subramanian *et al.* [11] have reviewed many developments in nanofluid simulation in a variety of technologies including chemical process engineering, materials fabrication, solar energy and lubrication systems. An important methodology for simulating nanoscale characteristics of nanofluids was introduced by Buongiorno [12], who developed a robust two-component model that includes both an energy balance and nanoparticle concentration balance, in addition to the momentum balance. The dominant transport mechanisms in this model are thermophoresis and Brownian dynamics. This model is accommodated comfortably in boundary layer theory and has been employed extensively in a wide spectrum of nanofluid dynamic transport problems. However, the Buongiorno model does not feature non-Newtonian characteristics, which have been confirmed *via* experimental studies by many researchers. For example, Hojjat *et al.* [13] have

studied γ-Al_2O_3, TiO_2 and CuO–aqueous carboxymethyl cellulose (CMC) nanofluids and have observed strong pseudoplastic (shear thinning) behaviour and also viscoelastic behaviour at different volume fractions. Other investigations identifying viscoelastic behaviour of nanofluids and nanopolymers include the work by Ghanbarpour *et al.* [14] and Sica *et al.* [15] for metallic and graphene nanoparticles in polymers, respectively. Therefore, to simulate the viscoelastic behaviour of nanofluids (nanopolymers), a pragmatic approach is the combination of the Buongiorno model with a robust non-Newtonian model. Rana *et al.* [16] utilized an HP-finite element method, Buongiorno's model and the Reiner–Rivlin second-grade non-Newtonian model to study the dissipative viscoelastic nanofluid transport from a stretching surface with energy dissipation effects. Vasu *et al.* [17] implemented HAM and modified differential quadrature schemes to examine the time-dependent magnetized viscoplastic Buongiorno nanoliquid boundary-layer flow from a stretched sheet doped with gyrotactic micro-organisms, as a model of bio–nanocoating dynamics. The Maxwell elastic–viscous model has however proved extremely popular in conjunction with the Buongiorno model for nanopolymeric materials processing analysis. Abbasi *et al.* [18] investigated the oblique stagnation bioconvection flow of a Maxwell nanofluid on a convective surface. They noted a strong depletion in the Nusselt number and Sherwood number with increasing Maxwell viscoelastic effects. Khan and Nadeem [19] used a bvp4c quadrature technique in MATLAB to compute the electrically conducting Maxwell nanofluid Hiemenz flow from a shrinking sheet (multiple solutions). Khan *et al.* [20] computed the Maxwell nanofluid stagnation point slip flow. Ahmed *et al.* [21] scrutinized the swirling flow induced by a rotating disk to a Maxwell nanoliquid with heat generation/absorption characteristics. Further studies of Maxwell nanofluid dynamics in materials processing systems concerning stretching surfaces include Ghasemian *et al.* [22], Bai *et al.* [23], Jagwal *et al.* [24], Ahmed *et al.* [25], Irfan *et al.* [26] and Acharya *et al.* [27]. All these analyses have confirmed the prominent effect of Maxwell viscoelasticity on transport characteristics and the inadequacy of a Newtonian model to capture the realistic behaviour of nanopolymer flows.

In nanopolymeric manufacturing processes, chemical reactions arise. These contribute to the polymerization and compatibilization processes and enable the generation of different compositions of the fabricated product. Many excellent experimental studies have examined such reactions in multiple polymeric materials including polyethylene blends [28], viscoelastic coatings [29] and polycarbonate/polyamide bilayer films synthesized from stretching surfaces [30]. Chemical reactions strongly influence heat and mass transport and very sophisticated interplays arise between the thermal, momentum and mass diffusion processes. Chemical reactions can be divided generally into two categories: homogeneous chemical reactions, which occur uniformly across a phase, and heterogeneous chemical reactions, which occur inside or near the boundary of the segment. First-order, higher-order and binary reactions are examples of homogenous chemical reactions. The presence of chemical reactions in nanofluid manufacturing has therefore motivated engineers and mathematicians to develop models that simulate robust chemo-nanofluid mechanics transport [31]. Newtonian reactive nanofluid flows were initially studied. Shukla *et al.* [32] conducted the second law thermodynamic analysis of the transient stagnation point flow of Newtonian reactive nanofluids from a stretching sheet under orthogonal electrical and magnetic fields with a finite element method. They observed that a stronger homogenous first-order chemical reaction suppresses entropy generation, whereas both the increasing electrical and magnetic field strength elevate the entropy generation. Garvandha *et al.* [33] employed a finite difference scheme to simulate phase change in the Buongiorno nanoliquid boundary-layer reactive flow induced by inclined stretched cylinder under curvature and cross-diffusion aspects. They observed a dramatic depletion in the nanoparticle concentration with greater order of the chemical reaction and a reduction in the concentration boundary layer thickness. Chemically reacting non-Newtonian flows have also received attention more recently. Adesanya *et al.* [33] considered third-grade viscoelastic reactive heat transfer in a channel. Shamshuddin *et al.* [34] and Kamran and Wiwatanapataphee [35] used Eringen's micropolar model to simulate reactive polymeric processing flows. Khan *et al.* [36] employed the Carreau–Yasuda rheological model with a chemical reaction and activation energy. Khan *et al.* [37] implemented the Casson viscoplastic model to study the reactive convection flow from a stretching vertical surface. Besides, reactive non-Newtonian nanoliquid flows have been investigated rigorously. Khan and Alzahrani [38] computed the Jeffrey viscoelastic nanofluid flow from a curved stretching surface with a binary chemical reaction, activation energy and viscous heating effects. The chemically reacting Maxwell viscoelastic nanofluid flow from a stretching cylinder was simulated using homotopy analysis by Irfan *et al.* [39], who observed that the mass transport rate (Sherwood number) for the constructive–destructive chemical reaction is opposite in nature to the response computed for the thermal Biot number.

In high-temperature polymeric materials processing systems, radiative heat transfer arises in addition to convection and conduction heat transfers [40]. Film stretching

processes often utilize radiative flux to manipulate heat transfer characteristics [41]. The general equation of radiative transfer is formidable to solve. In coupled radiative–convective–conductive flows, a simpler approach is required. Algebraic flux models are often used, and the popular ones among these (in order of increasing complexity) are the Rosseland diffusion flux model, Schuster–Schwartzchild two-flux model and Hamaker 6 flux model [42]. Rosseland's diffusion flux model is valid for optically thick fluids that can absorb or emit radiation at their boundaries and is quite accurate for most polymers [42]. However, it neglects scattering effects and is restricted to gray fluids. Many studies have featured this model in both non-Newtonian and Newtonian radiative polymeric flow simulations. Ramana Murthy *et al.* [43] studied the radiative heat flux effects on the entropy generation in a channel flow of two immiscible couple stress (polar) fluids. Janardhana Reddy *et al.* [44] used Rosseland's flux model and the Eringen micropolar rheological model to simulate the time-dependent thermal coating flow of an electroconductive polymer on a cylinder. Uddin *et al.* [45] used the Rosseland diffusion model to compute radiative flux effects on the nanofluid convection boundary layer flow from extending/retracting sheet surfaces. The Maxwell nanofluid flow from a convectively heated surface with the Rosseland radiative flux was investigated by Hayat *et al.* [46]. They observed that the temperature and boundary layer thickness are both elevated with a stronger thermal radiative effect, whereas the Nusselt number (rate of heat-transfer rate to the wall) is depleted. Akinbo and Olajuwon [47] scrutinized the chemically reacting viscoelastic magnetic boundary layer flow from a stretching sheet with Newtonian heating and Rosseland radiative flux. They observed that the flow is augmented (skin friction is increased) with a higher radiative effect and the Nusselt number is suppressed. The analysis of the Buongiorno nanofluid model considering the viscous fluid radiative flow was addressed by Mahanthesh [48]. His study discloses that the nanoparticles suspension upsurges thermal conductivity and, therefore, the heat flux at the surface decays while the temperature is augmented. Rana *et al.* [49] modeled the buoyancy-driven nanofluid slip flow subjected to thermal radiation. Their results illustrate that the nanofluid velocity improves due to quadratic thermal convection. The two-dimensional buoyancy-driven nanofluid convected flow with thermal radiation was investigated by Rana *et al.* [50]. Their analysis witnessed that radiation and nanoparticle aggregation aspects improve the temperature distribution. Sabu *et al.* [51] evaluated the thermally radiative magnetohydrodynamic nanomaterial flow under quadratic convection. They noticed that the heat-flux sensitivity towards inclination angle upsurges at a 0.5094% rate for higher radiation factors. The chemically reactive three-dimensional nanofluid radiative flow featuring Joule heating was examined by Swain and Mahanthesh [52]. They observed that the thermal field is improved significantly due to nanoparticles aggregation.

A review of the literature has revealed that thus far no study has examined the combined effects of the Maxwell viscoelastic behaviour, Rosseland radiative flux, wall transpiration, Newtonian heating and chemical reaction in a nonlinear rheological nanofluid flow from a stretching permeable surface. This is the novelty and focus of the present work. Both wall suction and injection cases are considered and heat generation/absorption is additionally included. The convective, thermal and solutal boundary conditions are utilized to provide a more comprehensive evaluation of temperature and concentration distributions. Buongiorno's nanofluid model featuring thermophoretic and Brownian motion effects is deployed. A first-order chemical reaction is considered. Dimensionless equations are used to create the flow model by utilizing the appropriate parameters. The computed models are presented through the convergent Liao homotopic analysis method (HAM) approach [53] with the help of Mathematica-12 symbolic software. Validation of HAM solutions with special cases from the literature is included. The impact of various thermophysical, nanoscale and rheological parameters (*e.g.* Deborash viscoelastic parameter, mixed convection parameter, chemical reaction parameter, *etc.*) on transport characteristics is visualized graphically and interpreted in detail. Convergence studies for HAM approximations are also included. The present study constitutes a novel contribution to the non-Newtonian reactive polymer processing simulation and has not been communicated thus far in the scientific literature.

2 Reactive viscoelastic nanofluid flow model

A steady, incompressible, non-Newtonian Maxwell nanofluid boundary layer flow towards a stretchable sheet surface is considered as a model for the nanopolymer flow processing. The sheet is oriented along the x-direction. The flow is limited to $y \geq 0$ and is visualized in Figure 1. It is presumed that $u_w(x) = cx$ is the stretchable surface velocity and $u_e(x) = ex$ is the external flow velocity where $c > 0$ and $e > 0$. The velocity field is defined by $V = [u(x, y), v(x, y), 0]$. The nanoparticles in the nanofluid are assumed to be chemically reacting and simulated using a first-order homogenous model. The nanofluid is

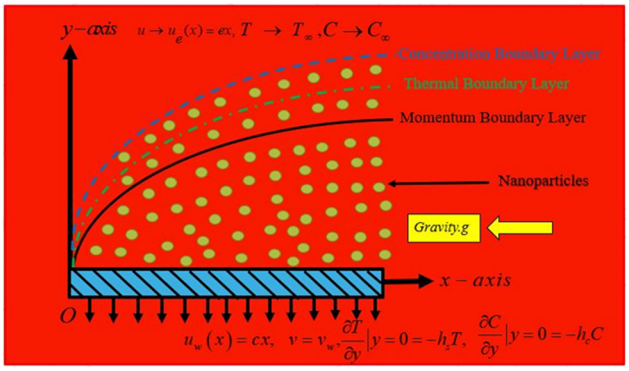

Figure 1: Physical model illustrating the reactive radiative–convective Maxwell nanofluid stretched flow.

also assumed to be optically thick and grey. The Rosseland radiation diffusion flux model is deployed to simulate thermal radiation and assumes that the intensity is the black-body intensity at the fluid temperature. Convective boundary conditions are applied at the wall (sheet) and transpiration (lateral masss flux) is present, *i.e.* suction injection. Under these approximations, the boundary layer approximation and the usual Boussinesq approximation, the governing conservation boundary layer equations for mass, momentum, energy and nanoparticle concentration, under thermosolutal buoyancy forces, may be derived by extending the analysis of Irfan *et al.* [39] to evaluate the radiative transfer, Newtonian heating and wall transpiration, as follows

$$\frac{\partial u}{\partial x} + \frac{\partial v}{\partial y} = 0, \tag{1}$$

$$\begin{cases} u\dfrac{\partial u}{\partial x} + v\dfrac{\partial u}{\partial y} + \lambda_1\left(u^2\dfrac{\partial^2 u}{\partial x^2} + v^2\dfrac{\partial^2 v}{\partial y^2} + 2uv\dfrac{\partial^2 u}{\partial x \partial y}\right) \\ \quad = \nu\dfrac{\partial^2 u}{\partial y^2} + u_e\dfrac{\mathrm{d}u_e}{\mathrm{d}x} \\ + g\{\Lambda_1(T - T_\infty) + \Lambda_2(T - T_\infty)^2\} \\ \quad + g\{\Lambda_3(C - C_\infty) + \Lambda_4(C - C_\infty)^2\}, \end{cases} \tag{2}$$

$$u\frac{\partial T}{\partial x} + v\frac{\partial T}{\partial y} = \alpha\frac{\partial^2 T}{\partial y^2} + \tau\left[D_B\frac{\partial C}{\partial y}\frac{\partial T}{\partial y} + \frac{D_T}{T_\infty}\left(\frac{\partial T}{\partial y}\right)^2\right] + \frac{16\sigma^* T_\infty^3}{3k^*}\frac{\partial^2 T}{\partial y^2}, \tag{3}$$

$$u\frac{\partial C}{\partial x} + v\frac{\partial C}{\partial y} = D_B\frac{\partial^2 C}{\partial y^2} + \frac{D_T}{T_\infty}\frac{\partial^2 T}{\partial y^2} - K_1(C - C_\infty). \tag{4}$$

The prescribed boundary conditions at the sheet (wall) and in the free stream take the form

$$u = u_w(x) = cx,\ v = v_w,\ \frac{\partial T}{\partial y} = -h_s T,\quad \frac{\partial C}{\partial y} = -h_c C \ \text{ at } \ y = 0, \tag{5}$$

$$u \to u_e(x) = ex,\ T \to T_\infty,\ C \to C_\infty \ \text{ when } \ y \to \infty. \tag{6}$$

Here, $\nu\left(=\frac{\mu}{\rho_f}\right)$ is the kinematic viscosity, ρ_f is the nanofluid (polymer) density, μ is the dynamic viscosity, λ_1 is the relaxation time, g is the gravitational acceleration, (Λ_1, Λ_3) denote the linear (thermal, concentration) expansion coefficients, (Λ_2, Λ_4) denote the nonlinear (thermal, concentration) expansion coefficients, $\alpha = \frac{k}{(\rho c)_f}$ is the thermal diffusivity, $\tau = \frac{(\rho c)_p}{(\rho c)_f}$ is the heat capacity ratio with $(\rho c)_f$ being the liquid heat capacity and $(\rho c)_p$ the nanoparticles' effective heat capacity, σ^* is the Stefan–Boltzmann constant, $(D_T,\ D_B)$ are (thermophoresis, Brownian) the diffusion coefficients, K_1 is the reaction rate, k^* is the coefficient of radiative mean absorption, $(T,\ C)$ is for the liquid (temperature, concentration), $u_w(x)$ is the stretching velocity, $u_e(x)$ is the free stream velocity, k is the thermal conductivity, c is the stretching rate, $(h_s,\ h_c)$ is the convective (heat, mass) transfer coefficient, $(T_\infty,\ C_\infty)$ is for the ambient liquid (temperature, concentration), respectively, and $(u,\ v)$ denote the components of velocity in the $(x,\ y)$ directions, respectively.

Introducing the following similarity variables [55]:

$$\begin{cases} \eta = y\sqrt{\dfrac{c}{\upsilon}},\ u = cxf'(\eta),\ v = -\sqrt{c\upsilon}f(\eta), \\ \theta(\eta) = \dfrac{T - T_\infty}{T_\infty},\ \phi(\eta) = \dfrac{C - C_\infty}{C_\infty}. \end{cases} \tag{7}$$

Equation (1) is fulfilled automatically. Equations (2)–(6) reduce to the following self-similar momentum, thermal and concentration boundary layer equations with associated boundary conditions:

$$f''' + f f'' + \beta(2f f' f'' - f^2 f''') - (f')^2 + \delta[(1 + \beta_t\theta)\theta + N(1 + \beta_c\phi)\phi] + A^2 = 0, \tag{8}$$

$$\left(1 + \frac{4}{3}R\right)\theta'' + \mathrm{Pr}f\theta' + \mathrm{Pr}(N_t\theta'^2 + N_b\phi'\theta') = 0, \tag{9}$$

$$\phi'' + \mathrm{Sc}(f\phi' - \gamma\phi) + \frac{N_t}{N_b}\theta'' = 0, \tag{10}$$

$$\begin{cases} \text{at } \eta = 0,\ f = S,\ f' = 1,\ \phi = -\gamma_2(1 + \phi(\eta)), \\ \theta = -\gamma_1(1 + \theta(\eta))\,, \\ \text{as } \eta \to \infty,\ f' \to A,\ \phi \to 0\,,\ \theta \to 0\,. \end{cases} \tag{11}$$

Here (′) designates differentiation with respect to the transformed dimensionless y-coordinate, *i.e.* η, β is the Deborah (viscoelastic) number, δ is the mixed convection variable, Gr_x is the local thermal Grashof number (thermal buoyancy parameter), N is the ratio of concentration/thermal buoyancy, Gr_x^* is the local solutal Grashof number (solutal buoyancy parameter), (β_t, β_c) are nonlinear (thermal, concentration) convection variable quantities, A is the ratio of free stream velocity/stretching velocity, S denotes the wall lateral mass flux parameter:for suction ($S > 0$) or for injection ($S < 0$), N_t is a thermophoresis variable, Pr is the Prandtl number, (γ_1, γ_2) denotes the conjugate (heat, mass) transfer, $R$is a radiation parameter, N_b is a Brownian motion parameter: ($\gamma > 0$) for generative chemical reaction and ($\gamma < 0$) for destructive chemical reaction and Sc is the Schmidt number. These variables are defined as follows:

$$\begin{aligned}
&\beta = \lambda_1 c,\ \delta = \frac{\mathrm{Gr}_x}{\mathrm{Re}_x^2},\ \mathrm{Gr}_x = \frac{g\Lambda_1 T_\infty x^3}{\upsilon^2},\\
&\mathrm{Gr}_x^* = \frac{g\Lambda_3 C_\infty x^3}{\upsilon^2},\\
&\beta_t = \frac{\Lambda_2 T_\infty}{\Lambda_1},\ \beta_c = \frac{\Lambda_4 C_\infty}{\Lambda_3},\ N = \frac{\mathrm{Gr}_x^*}{\mathrm{Gr}_x},\ \mathrm{Re}_x = \frac{x u_w}{\upsilon},\\
&S = \frac{v_w}{\sqrt{c\upsilon}},\\
&N_t = \frac{\tau D_T}{T_\infty \upsilon},\ A = \frac{e}{c},\ \mathrm{Pr} = \frac{\upsilon}{\alpha},\ N_b = \frac{\tau D_B}{\upsilon},\ \gamma = \frac{K_1}{c},\\
&R = \frac{4\sigma^* T_\infty^3}{kk^*},\ \mathrm{Sc} = \frac{\upsilon}{D_B},\ \gamma_1 = h_s\sqrt{\frac{\upsilon}{c}},\ \gamma_2 = h_c\sqrt{\frac{\upsilon}{c}}.
\end{aligned} \tag{12}$$

The heat transfer rate and mass (concentration) transfer rate may be expressed using local Nusselt and Sherwood numbers, which take the following definitions:

$$\mathrm{Nu}_x = -\frac{x q_w}{k(T - T_\infty)},\ q_w = -\left(k + \frac{16\sigma^* T_\infty^3}{3k^*}\right)\left(\frac{\partial T}{\partial y}\right)_{y=0}, \tag{13}$$

$$\mathrm{Sh}_x = -\frac{x j_w}{D_B(C - C_\infty)},\ j_w = -D_B\left(\frac{\partial C}{\partial y}\right)_{y=0}. \tag{14}$$

In non-dimensional form, using the transformations defined in equation (7) the desired expressions are as follows:

$$\mathrm{Nu}_x \mathrm{Re}_x^{-0.5} = \gamma_1\left(1 + \frac{4}{3}R\right)\left(1 + \frac{1}{\theta(0)}\right), \tag{15}$$

$$\mathrm{Sh}_x \mathrm{Re}_x^{-0.5} = \gamma_2\left(1 + \frac{1}{\phi(0)}\right). \tag{16}$$

Here, Re_x denotes the local Reynolds number based on the coordinate x.

3 Homotopy analysis method (HAM) solutions and convergence

To solve the nonlinear transformed boundary value problem, defined by equations (8)–(11), the powerful semi-analytical power series expansion technique known as HAM is implemented [48]. This method achieves exceptional accuracy and can successfully accommodate nonlinear fluid mechanics simulations. It has been used to study Maxwell viscoelastic flows [54], Carreau reactive flows [55], thermosolutal transport in porous media [56], biological propulsion of Oldroyd-B liquids [57] and magneto-tribological micropolar flows [58]. For the present problem, the initial guesses $(f_0(\eta),\ \theta_0(\eta),\ \phi_0(\eta))$ and auxiliary linear operators $(L_f,\ L_\theta,\ L_\phi)$ are defined as follows:

$$\begin{aligned}
f_0(\eta) &= S + A \times \eta + (1 - A)(1 - \mathrm{e}^{-\eta}),\\
\theta_0(\eta) &= \left(\frac{\gamma_1}{1 - \gamma_1}\right) \times \mathrm{e}^{-\eta},\\
\phi_0(\eta) &= \left(\frac{\gamma_2}{1 - \gamma_2}\right) \times \mathrm{e}^{-\eta},
\end{aligned} \tag{17}$$

$$\begin{cases}
L_f = f''' - f',\\
L_\theta = \theta'' - \theta,\\
L_\phi = \phi'' - \phi,
\end{cases} \tag{18}$$

with

$$\begin{cases}
L_f(A_1 + A_2\mathrm{e}^{\eta} + A_3\mathrm{e}^{-\eta}) = 0,\\
L_\theta(A_4\mathrm{e}^{\eta} + A_5\mathrm{e}^{-\eta}) = 0,\\
L_\phi(A_6\mathrm{e}^{\eta} + A_7\mathrm{e}^{-\eta}) = 0,
\end{cases} \tag{19}$$

Here, $C_i(i = 1 - 7)$ denote the arbitrary constants.

HAM is utilized to identify solutions in terms of convergence. This method involves an auxiliary parameter $\hbar$,

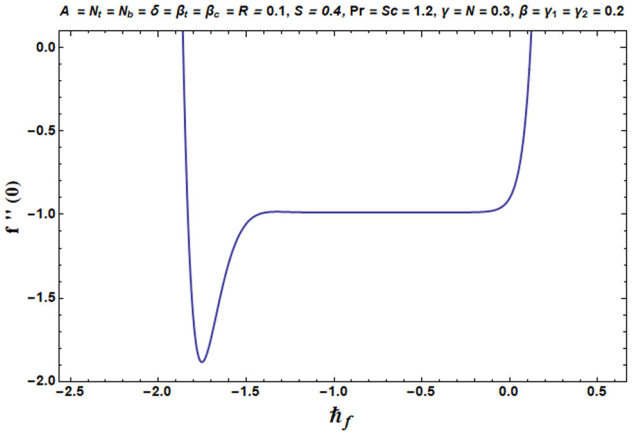

Figure 2: *H* curve stimulus for $f''(0)$.

which facilitates us to modify the convergence area of $f''(0), \theta'(0), \phi'(0)$ The supplementary parameter h demonstrates a critical role. Figures 2–4 show the "h curves". It is observed that the approved values of h_f, h_θ and h_ϕ in Figures 2–4 are $-1.4 \le h_f \le -0.2$, $-1.3 \le h_\theta \le -0.1$ and $-1.3 \le h_\phi \le -0.1$. The convergences of velocity gradient $f''(0)$, temperature gradient $\theta'(0)$ and concentration gradient $\phi'(0)$ are presented in Table 1. It is evident that the 35th order of approximations is appropriate for $f''(0)$ and $\theta'(0)$, whereas the 25th order of approximation is necessary for $\phi'(0)$.

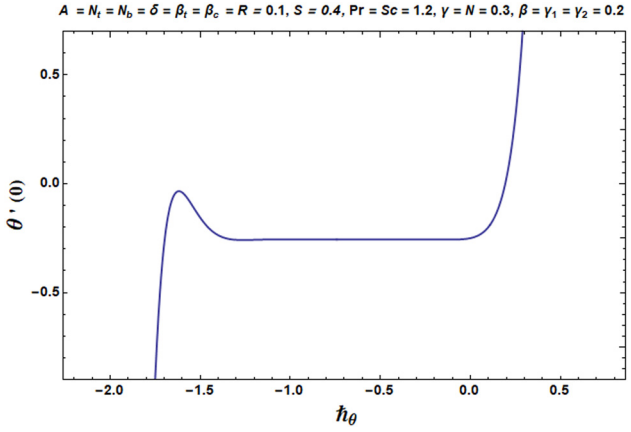

Figure 3: H curve stimulus for $\theta'(0)$.

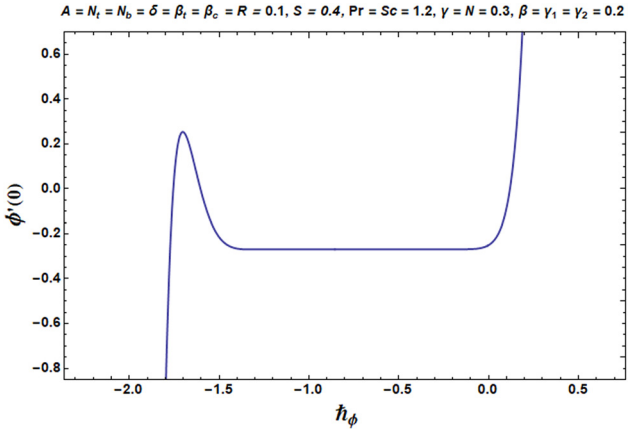

Figure 4: H curve stimulus for $\phi'(0)$.

4 Authentication of HAM solutions

To validate the correctness of HAM computations, a comparison with several earlier studies from the literature is conducted. The comparison results of the skin friction coefficient in a limiting case agree very closely with the literature as displayed in Tables 2 and 3. Confidence in the present HAM solutions is therefore justifiably very high.

5 Analysis of results

Extensive HAM calculations have been conducted and are shown in Figures 5–19.

Figures 5–9 depict the velocity evolution $f'(\eta)$ with the variations in A (ratio of the external velocity/stretching rate velocity, *i.e.* $\frac{e}{c}$), β (Deborah number), δ (mixed convection parameter), S (suction/injection parameter) and N (ratio of the concentration/thermal buoyancy force parameter). Figure 5 indicates that with increment in the velocity ratio, A, $f'(\eta)$ experiences a strong enhancement, *i.e.* the flow is accelerated. When ($A > 1$), the stream velocity (e) exceeds the linear velocity of the sheet stretching (c). This induces a momentum boost *via* the external free stream that

Table 1: Convergence of HAM series solution when $A = \delta = N_t = N_b = \beta_t = \beta_c = R = 0.1$, $S = 0.4$, $N = \gamma = 0.3$, $\Pr = Sc = 1.2$, $\beta = \gamma_1 = \gamma_2 = 0.2$

Order of approximations	$-f''(0)$	$-\theta'(0)$	$-\phi'(0)$
5	0.95931	0.2555	0.2646
10	0.97804	0.2567	0.2684
15	0.98427	0.2565	0.2689
20	0.98650	0.2562	0.2690
25	0.98734	0.2560	0.2690
30	0.98766	0.2559	0.2690
35	0.98780	0.2558	0.2690
40	0.98780	0.2558	0.2690
45	0.98780	0.2558	0.2690

Table 2: Comparison of $f''(0)$ with the works of Ramesh *et al.* [59], Hayat *et al.* [60], Panigrahi *et al.* [61], Mathew *et al.* [62], and Akinbo and Olajuwon [47] in the limiting case when $\beta = \delta = 0$

A	Ramesh *et al.* [59]	Hayat *et al.* [60]	Panigrahi *et al.* [61]	Mathew *et al.* [62]	Akinbo and Olajuwon [47]	Present study (HAM)
0.01	−0.9991	—	—	—	—	−0.9980
0.1	−0.9696	−0.96937	−0.969385	−0.9693861	−0.96801	−0.96939
0.2	−0.9181	−0.91813	−0.918106	−0.9181071	−0.91688	−0.91811
0.5	−0.6672	−0.66723	−0.667263	−0.6672637	−0.66716	−0.66726
2.0	2.0175	—	2.0175001	—	2.01750	—
3.0	4.7292	—	4.729277	—	4.72917	—
0.7	—	−0.43345		−0.4334755	—	−0.43347
0.8	—	−0.29921		−0.299388	—	−0.299388
0.9	—	−0.1545471		−0.1547167	—	−0.154716
1.0		0		0	—	0

Table 3: Comparison of $f''(0)$ with the works of Abel *et al.* [63], Megahed [64], Irfan *et al.* [39], and Ujjini Bhojappa and Zeb [65] in the limiting case when $A = \delta = 0$

β	Abel *et al.* [63]	Megahed [64]	Irfan *et al.* [39]	Ujjini Bhojappa and Zeb [65]	Present study (HAM)
0.0	−1.0000	−0.999978	−1.0000	−1.0000	−1.0000
0.2	−1.051948	−1.051945	−1.051890	−1.051889	−1.0519
0.4	−1.1019	−1.1019	−1.1019	−1.101898	−1.1019
0.6	−1.1501	−1.1501	−1.1501	−1.150128	−1.1501
0.8	−1.1968	−1.1968	−1.1968	−1.196708	−1.1967
1.2	−1.2854	−1.2854	−1.2854	−1.285361	−1.2854
1.6	−1.3686	−1.3686	−1.3686	−1.368757	−1.3688
2.0	−1.4476	−1.4476	−1.4476	−1.447648	−1.4476

manifests in strong acceleration at all values of transverse coordinates, η. The momentum (hydrodynamic) boundary layer thickness is therefore reduced. However, for $(A < 1)$, the stretching velocity exceeds the external free stream velocity and the opposite effect is computed, *i.e.* the velocity $f'(\eta)$ is suppressed and the boundary layer thickness increases. When $(A = 1)$, both external and stretching velocities are equal and this case naturally falls between the other two cases of $A > 1$ and $A < 1$. Clearly, greater stretching of the sheet is inhibitive to the momentum development, whereas a greater external velocity is assistive. A reflective symmetry is computed about the line

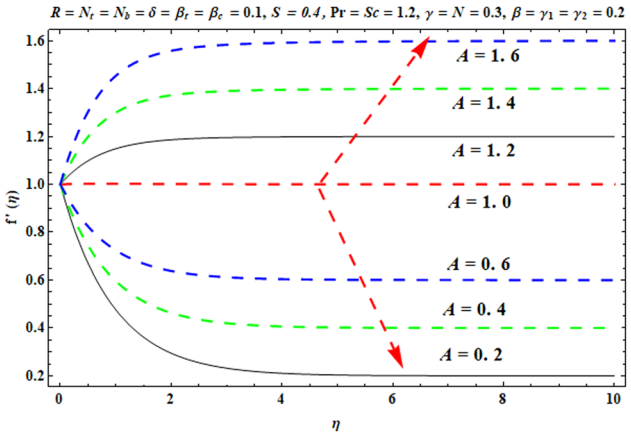

Figure 5: $f'(\eta)$ *versus* A.

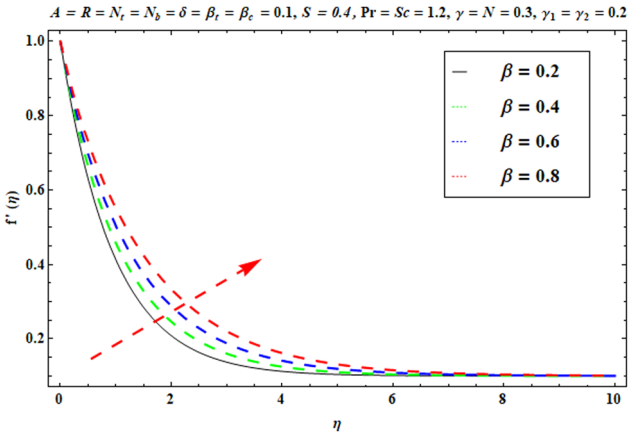

Figure 6: $f'(\eta)$ *versus* β.

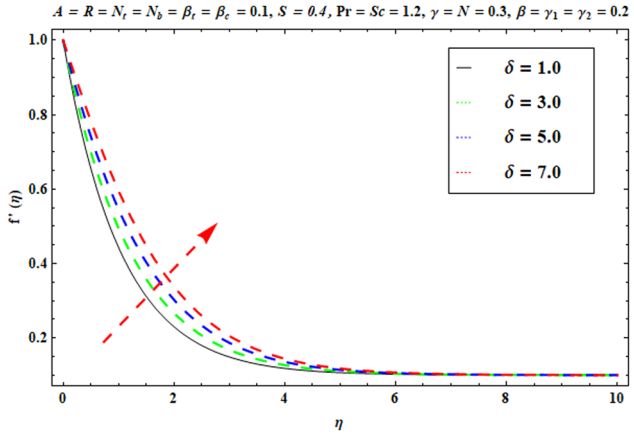

Figure 7: $f'(\eta)$ *versus* δ.

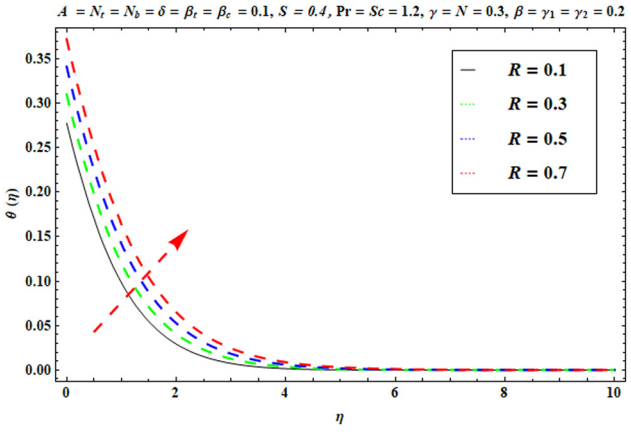

Figure 10: $\theta(\eta)$ *versus* R.

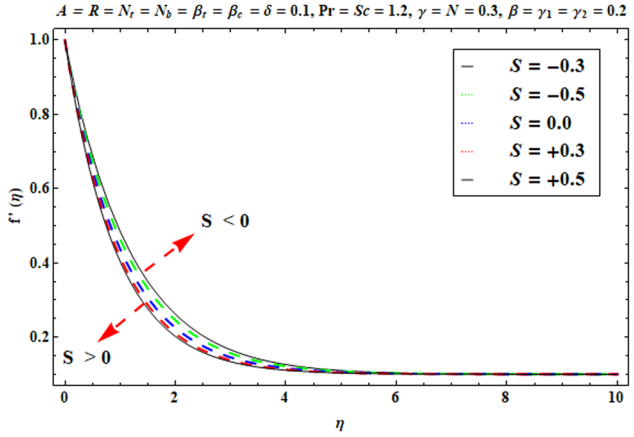

Figure 8: $f'(\eta)$ *versus* S.

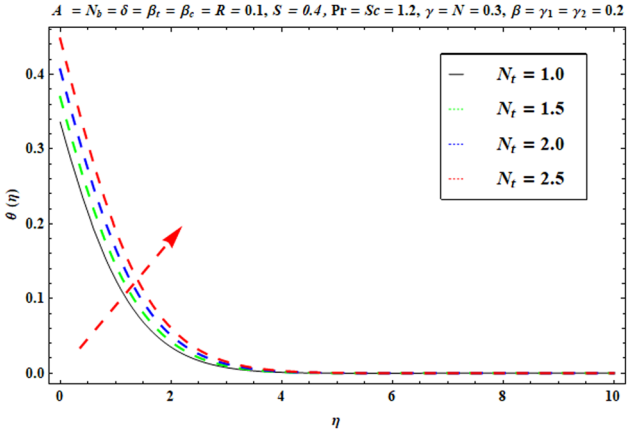

Figure 11: $\theta(\eta)$ *versus* N_t.

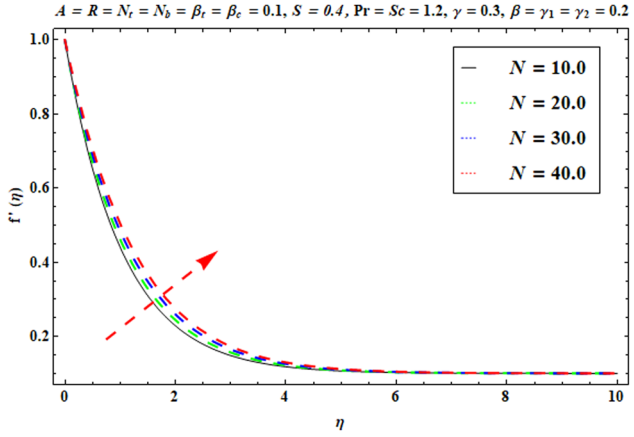

Figure 9: $f'(\eta)$ *versus* N.

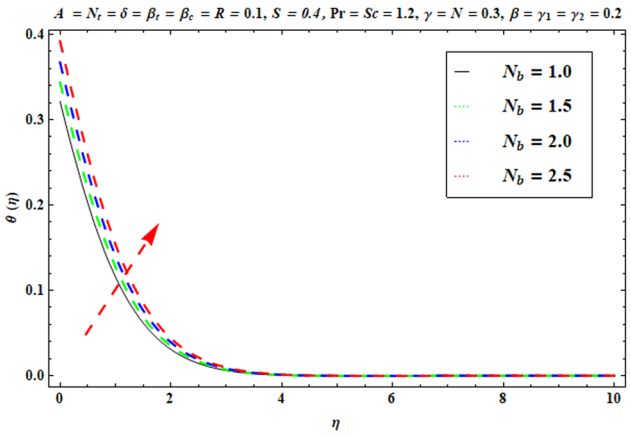

Figure 12: $\theta(\eta)$ *versus* N_b.

$A = 0$ for $A < 1$ and $A < 1$. Figure 6. exhibits the influence of β on $f'(\eta)$ and a substantial elevation in velocity is witnessed with greater values of the Deborah number. This parameter arises in the augmented shear terms in the momentum boundary layer equation (8), *viz* $+\beta(2ff'f'' - f^2f''')$. $\beta = \lambda_1 c$ and larger values of this parameter

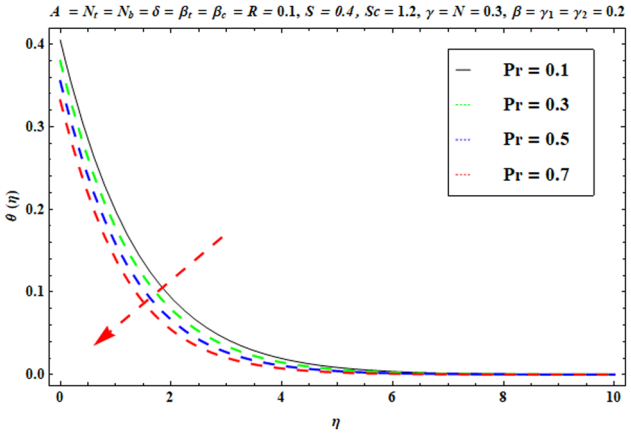

Figure 13: $\theta(\eta)$ *versus* Pr.

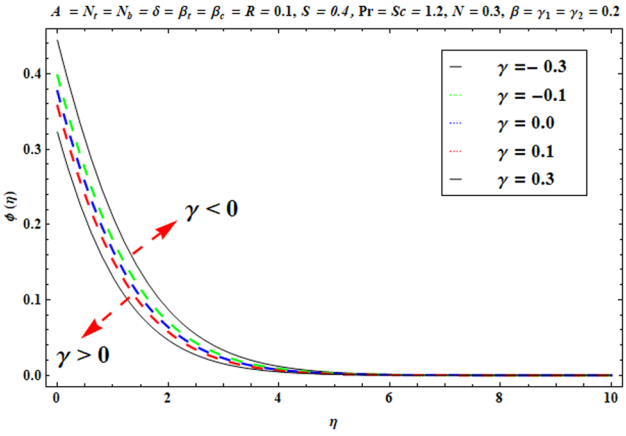

Figure 16: $\phi(\eta)$ *versus* γ.

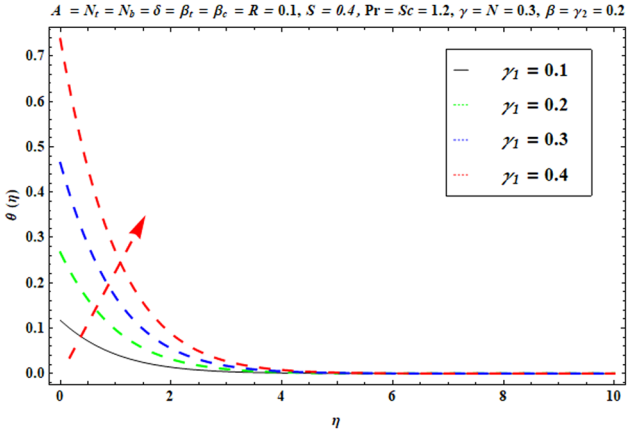

Figure 14: $\theta(\eta)$ *versus* γ_1.

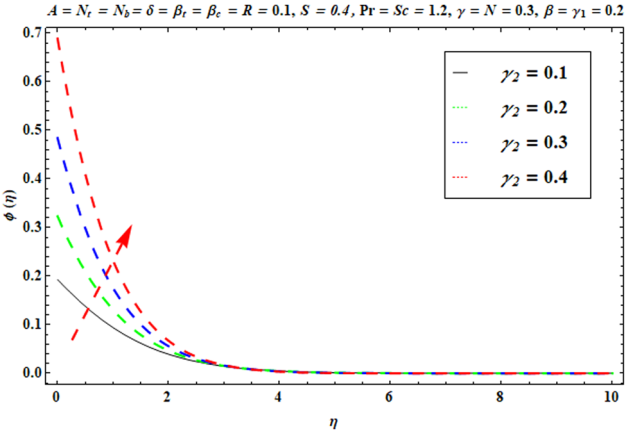

Figure 17: $\phi(\eta)$ *versus* γ_2.

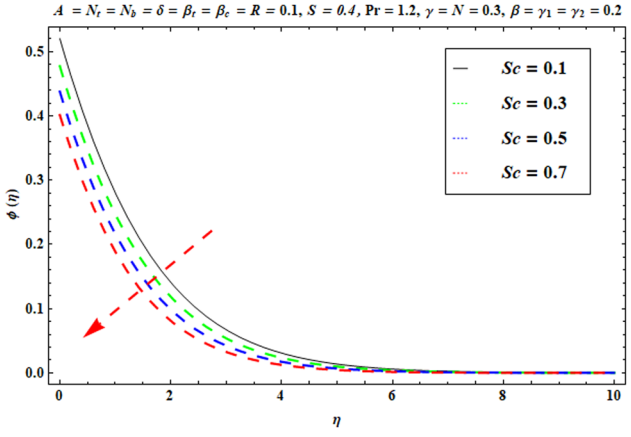

Figure 15: $\phi(\eta)$ *versus* Sc.

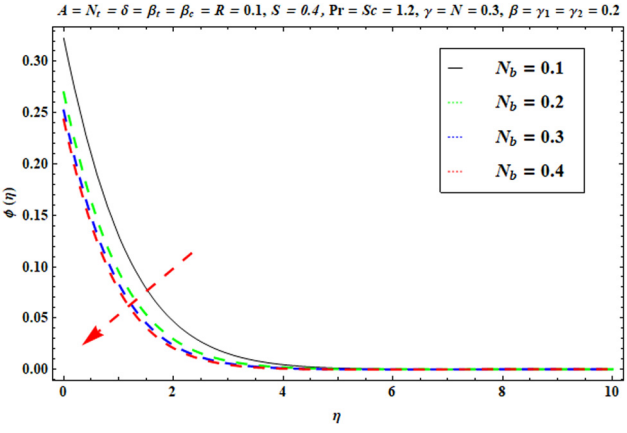

Figure 18: $\phi(\eta)$ *versus* N_b.

correspond to greater viscous effects and lower elasticity in the nanofluid polymer. This also implies a greater relaxation time of the nanofluid that assists momentum diffusion and accelerates the flow. The momentum boundary-layer thickness is consequently diminished with higher Deborah number values. The inclusion of a viscoelastic rheological

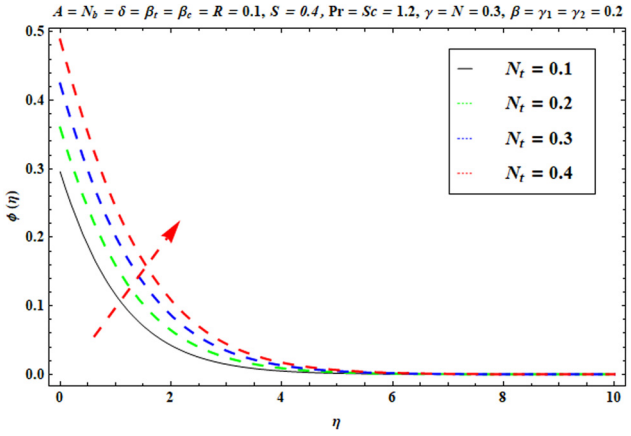

Figure 19: $\phi(\eta)$ *versus* N_t.

model is therefore important since it captures acceleration effects, which would be neglected with Newtonian modelling in which the velocity is under-predicted. Figure 7 implies that with greater values of mixed convection variables δ, there is also an upsurge of velocity $f'(\eta)$. Clearly, the thermal buoyancy force is intensified with greater values of $\delta = \frac{(Gr_x)}{(Re_x^2)}$. This energizes the nanopolymer boundary-layer regime and the flow is accelerated leading to a reduction in the momentum boundary-layer thickness. Figure 8 illustrates that with the increment in wall suction ($S > 0$), there is depletion in velocity magnitudes. Flow deceleration is induced since the nanopolymer boundary layer adheres more strongly to the wall and the momentum is reduced. The hydrodynamic boundary layer thickness is thereby enhanced in the regime. However, velocities are always positive, *i.e.* no flow reversal or separation is induced in the boundary layer. Conversely with increment in the injection factor ($S < 0$), there is a boost in the velocity owing to the introduction of greater momentum in the regime *via* blowing through the porous (permeable) stretching sheet. This accelerates the nanopolymer boundary layer flow and leads to a thinner momentum boundary layer thickness. With greater values of the species/thermal buoyancy ratio, N, a significant elevation in velocity occurs throughout the regime (see Figure 9). In all cases, $N \gg 1$ implies that the nanoparticles' species buoyancy force greatly exceeds the thermal buoyancy force. This generates a reduction in the momentum boundary layer thickness. In all the plots, asymptotically smooth profiles are achieved in the free stream, confirming that a sufficiently high value is prescribed in HAM computations for the infinity boundary condition.

Figures 10–14 illustrate the influence of the radiation parameter, R, on the thermophoresis variable, N_t on the Brownian motion variable, N_b on the Prandtl number, Pr and the conjugate heat transfer γ_1, respectively, on temperature profiles, $\theta(\eta)$. Figure 10 shows clearly that when R increases, $\theta(\eta)$ is significantly enhanced. A stronger radiative flux energizes the stretching nanopolymer regime and augments thermal diffusion. Moreover, it manifests a growth in the thermal boundary-layer thickness. Physically, the presence of stronger thermal radiation (higher R values) generates greater heat (thermal energy). Therefore, neglecting the radiative transfer would lead to an under-prediction in the temperature computed in the nanopolymer flow processing. Figure 11 indicates that with greater values of the nanoscale thermophoresis parameter, N_t, there is an upsurge in the temperature, $\theta(\eta)$. Greater mobility of nanoparticles towards colder zones in the boundary layer regime is induced under a temperature gradient with a stronger thermophoretic body force. This exacerbates thermodiffusion in the regime and heats the boundary layer, resulting in a greater thermal boundary-layer thickness. Maximum temperatures for any case examined always however arise at the wall, *i.e.* the sheet and all profiles decay monotonically to the free stream. Figure 12 demonstrates that with increment in the Brownian motion parameter N_b, the temperature $\theta(\eta)$ is also elevated substantially. The intensification in ballistic collisions with greater Brownian motion effect leads to dissipation of the kinetic energy as thermal energy. This heats the regime and also enhances the thermal boundary layer thickness. Larger Nb values in the Buongiorno model imply smaller diameter spherical nanoparticles. There is an upsurge in the volume fraction, which leads to an exacerbation in chaotic nanoparticle collisions. The temperature of the nanopolymer can therefore be successfully manipulated with a change in the dimensions of the nanoparticles, as noted lucidly in Das *et al.* [9]. Nanopolymer constitution therefore exerts a significant role in the thermal field. With the increment in the Prandtl number, Pr, the temperature $\theta(\eta)$ is depleted. The Prandtl number expresses the relative rate of momentum diffusion to thermal diffusion in the boundary layer. It also expresses the ratio of the momentum boundary layer thickness/thermal boundary layer thickness. For Pr < 1, the energy diffusion rate exceeds the momentum (viscous) diffusion rate. An increment in the Prandtl number also implies a decrease in the thermal conductivity of the nanopolymer. This suppresses thermal convection in the boundary layer and decreases the temperature, *i.e.* induces a cooling effect. The effective Prandtl number of the nanopolymer can be manipulated by the selection of appropriate nanoparticles to modify thermal characteristics. Figure 14 reveals that with an upsurge in the conjugate thermal parameter γ_1 , there is an enhancement in the temperature, $\theta(\eta)$. Additionally, the gradient of the temperature plot is strongly modified at the wall and it is reduced with greater values of the conjugate

parameter. This effect is simulated *via* the modified convective boundary condition $\theta = -\gamma_1(1 + \theta(\eta))$ featuring in equation (11), which quantifies the strength of Newtonian heating. Clearly, neglecting this effect prevents the correct near-wall thermal distribution from being computed accurately. The rate of change of temperature with the transverse coordinate cannot be simulated properly at the sheet surface and in proximity to it without a Newtonian heating condition. Stronger Newtonian heating produces a greater thermal boundary layer thickness than the conventional thermal boundary conditions at the wall. These trends have also been observed in a number of other investigations including Kamran *et al.* [35] and Khan *et al.* [37]. Again, it is noteworthy that the correct asymptotic profiles in the free stream are computed in all temperature distributions confirming that an adequately large infinity boundary condition has been deployed in the HAM analysis.

Figures 15–19 show the impact of the Schmidt number Sc, chemical reaction parameter γ, conjugate mass transfer parameter γ_2 , Brownian motion parameter N_b, and thermophoresis parameter N_t on the dimensionless nanoparticle concentration, $\phi(\eta)$. Figure 15 implies that with an increase in Sc, there is a distinct depletion in the concentration profile $\phi(\eta)$. This is accompanied with a decrease in the species boundary layer thickness. Physically, Sc is inversely proportional to the molecular (mass) diffusivity of the nanoparticles in the polymer base fluid. As Sc increases, the molecular diffusion rate decreases and this inhibits the transport of nanoparticles in the boundary layer regime. The concentration magnitudes are therefore reduced. Manipulation of the distribution of nanoparticles in the resulting nanopolymer can be achieved therefore by judicious selection of nanoparticles with a particular diffusivity. Nanopolymers can therefore be effectively engineered using carefully selected nanoparticles [9]. Figure 16 shows that with a greater destructive chemical reaction factor $\gamma > 0$, the concentration $\phi(\eta)$ is depleted since a greater quantity of the original nanoparticles is converted to another species. The opposite trend is induced with a stronger generative (constructive) chemical reaction $\gamma < 0$ for which concentrations are increased and species boundary layer thickness is also elevated. The case of non-reactive flow ($\gamma = 0$) falls between these two types of chemical reactions. A homogenous chemical reaction is simulated *via* the first-order term, $+\mathrm{Sc}(-\gamma\phi)$ in the species boundary layer equation (10). This term becomes assistive (positive) for $\gamma < 0$ and inhibitive (negative) for $\gamma > 0$. Clearly, when the first-order homogenous chemical reaction is neglected in the model, this either under-predicts the concentration or overpredicts the concentration magnitudes, depending on whether destructive or constructive chemical reactions are being considered in nanopolymer processing. Figure 17 shows that as conjugate solutal (mass transfer) parameter γ_2 is increased, there is a boost in the magnitudes of the concentration of nanoparticles $\phi(\eta)$. This parameter arises in the augmented wall concentration boundary condition (11), *i.e.* $\phi = -\gamma_2(1 + \phi(\eta))$. Higher values of γ_2 strongly increase the dimensionless concentration $\phi(\eta)$ and simultaneously reduce the concentration gradient at and near the wall. An upsurge in the species, *i.e.* the solutal boundary layer thickness is therefore produced with the stronger conjugate mass transfer effect. Figures 18 and 19 show that the elevation in thermophoresis N_t and Brownian motion N_b

Table 4: Numerical values of the Nusselt number $\mathrm{Nu}_x\,\mathrm{Re}_x^{-\frac{1}{2}}$ when $A < 1$

Pr	R	N_b	N_t	A	β	δ	N	γ_1	$\mathrm{Nu}_x\mathrm{Re}_x^{-\frac{1}{2}}$
1.3	0.1	0.1	0.1	0.1	0.2	0.1	0.3	0.2	1.101
1.4									1.163
1.5									1.223
1.2	0.2								1.069
	0.3								1.098
	0.1	0.2							1.026
		0.3							1.014
		0.1	0.2						1.019
			0.3						0.9990
			0.1	0.2					1.059
				0.3					1.080
				0.1	0.3				1.054
					0.4				1.067
					0.2	0.2			1.041
						0.3			1.044
						0.1	0.4		1.039
							0.5		1.039
							0.3	0.3	1.025
								0.4	1.008

Table 5: Numerical values of the Sherwood number $\mathrm{Sh}_x\mathrm{Re}_x^{-\frac{1}{2}}$

Sc	γ	N_b	N_t	γ_2	$\mathrm{Sh}_x\mathrm{Re}_x^{-\frac{1}{2}}$
1.3	0.3	0.1	0.1	0.2	0.8218
1.4					0.8635
1.5					0.9047
1.2	0.1				0.6838
	0.2				0.7325
	0.3	0.2			0.9433
		0.3			1.0210
		0.1	0.2		0.6036
			0.3		0.5101
			0.1	0.3	0.9141
				0.4	1.0000

parameters, respectively, elevate and reduce $\phi(\eta)$. The intensified migration of nanoparticles under a thermophoretic body force results in a more homogenous distribution of nanoparticles and a higher concentration value. However, greater chaotic motion *via* Brownian motion produces more ballistic collisions that inhibit nanoparticle migration and reduce their concentration and also the species boundary layer thickness in the viscoelastic nanopolymer.

Table 4 shows the local Nusselt number $\mathrm{Nu}_x\,\mathrm{Re}_x^{-\frac{1}{2}}$ values for selected parameters Pr, R, N_b, N_t, A, β, δ, N and γ_1 when $\beta_t = \beta_c = 0.1$, $S = 0.4$, $\gamma = 0.3$, $\mathrm{Sc} = 1.2$, $\gamma_2 = 0.2$. Here $A < 1$, *i.e.* the stretching velocity exceeds the external velocity. The local Nusselt number magnitudes clearly increase, *i.e.* the heat transfer rate to the wall improves with elevation in Pr, R, A, β and δ, whereas they are reduced with increment in γ_1, N_b, N_t. Further, it is noticed that the parameter N does not significantly modify the heat transfer rate to the wall (porous sheet). Table 5 exhibits the local Sherwood number values $\mathrm{Sh}_x\,\mathrm{Re}_x^{-\frac{1}{2}}$ for various selected parameters. It is evident that the mass transfer rate to the wall is enhanced with greater values of Sc, γ and γ_2, whereas it is depleted with increment in N_t, N_b.

6 Conclusions

Inspired by the recent developments in high-temperature nanopolymeric materials processing, a theoretical study has been presented to investigate the combined effects of the chemical reaction and radiative heat flux in a nonlinear mixed thermosolutal convection flow of a viscoelastic nanoliquid from a stretchable surface theoretically. Newtonian heating (modified thermal convective boundary conditions) has also been included. The upper-convected Maxwell (UCM) model has been deployed to represent non-Newtonian characteristics. The model also includes the influence of thermal radiation, which is simulated *via* an algebraic flux model. Buongiorno's two-component nanofluid model has been implemented for thermophorestic and Brownian motion effects. The transformed, self-similar nonlinear boundary layer flow model with appropriate wall and free stream conditions has been solved with a convergent homotopic analysis method (HAM) approach with the help of Mathematica-12 symbolic software. Validation of HAM solutions with special cases from the literature has been included. A detailed parametric analysis highlighting the influence of all thermophysical, rheological and nanoscale factors on transport attributes has been elaborated. The principal findings of the present simulations can be summarized as follows:

1) Temperatures are strongly enhanced with the Brownian motion and thermophoresis parameter.
2) Velocity is boosted with increment in the Deborah viscoelastic number, and the mixed convection parameter and hydrodynamic boundary layer thickness are reduced.
3) Stronger generative chemical reaction enhances concentration magnitudes, whereas an increment in the destructive chemical reaction reduces them and also depletes the concentration boundary layer thickness.
4) Temperature is elevated with the conjugate thermal parameter and thermal boundary layer thickness is increased.
5) Nanoparticle concentration is boosted with greater values of the conjugate solutal parameter with an accompanying increase in the solutal boundary-layer thickness.
6) Greater radiative flux strongly upsurges the temperature and allied thermal boundary-layer thickness.
7) Stronger suction at the wall depletes velocity and increases the momentum boundary-layer thickness. However, an opposite result is induced for greater injection (blowing).
8) Higher external velocity relative to the stretching velocity induces strong flow acceleration, whereas the opposite case induces strong flow deceleration.
9) Increasing the Schmidt number and Brownian motion parameter diminishes the concentration values, whereas they elevate the local Sherwood number magnitudes, *i.e.* enhance the nanoparticle mass transfer rate to the wall.
10) Local Nusselt number magnitudes are boosted with elevation in the thermal buoyancy factor and Prandtl number, while they are suppressed with a greater conjugate thermal parameter, thermophoresis and Brownian motion parameter values.

Excellent stability, convergence and accuracy are achieved with HAM in nanopolymeric viscoelastic thermal flow processing simulation. The present study has neglected unsteady flow effects and also has been restricted to a single non-Newtonian model. Future investigations may consider time-dependent flow and other rheological models, *e.g.* Eringen's micropolar model and the Oldroyd-B viscoelastic model. HAM appears to be an excellent tool for simulating such flows.

Acknowledgments: D. Baba Basha would like to thank the Deanship of Scientific research at Majmaah

University for funding this work under project number No. R-2022-57.

Funding information: D. Baba Basha would like to thank the Deanship of Scientific research at Majmaah University for funding this work under project number No. R-2022-57.

Author contributions: All authors have accepted responsibility for the entire content of this manuscript and approved its submission.

Conflict of interest: The authors state no conflict of interest.

References

[1] Faith A, Morrison. Understanding rheology. Oxford: Oxford University Press; 2001.
[2] Dong Z, Ya G, Liu J. Study on machining mechanism of high viscoelastic abrasive flow machining for surface finishing. Proc Inst Mech Eng Part B J Eng Manufacture. 2015;231(4):608–17.
[3] Ahmadian Yazdi A, Sadeghi A, Saidi MH. Rheology effects on cross-stream diffusion in a Y-shaped micromixer. Colloids Surf A: Physicochem Eng Asp. 2014;456:296–306.
[4] Zhang W, Silvi N, Vlachopoulos J. Modelling and experiments of squeezing flow of polymer melts. Int Polym Process. 2013;10(2):1–9.
[5] Villone MM, Hulsen MA, Maffettone PL. Numerical simulations of viscoelastic film stretching and retraction. J Non-Newtonian Fluid Mech. 2019;266:118–26.
[6] Huang KH, Tsai R, Huang CH. Chebyshev finite difference approach to modeling the thermoviscosity effect in a power-law liquid film on an unsteady stretching surface. J Non-Newtonian Fluid Mech. 2010;165:1351–6.
[7] Anwar Bég O, Zueco J, Ghosh SK. Unsteady natural convection of a short-memory viscoelastic fluid in a non-Darcian regime: network simulation. Chem Eng Commun. 2010;198:172–90.
[8] Shahid A, Bhatti MM, Anwar Bég O, Kadir A. Numerical study of radiative Maxwell viscoelastic magnetized flow from a stretching permeable sheet with the Cattaneo–Christov heat flux model. Neural Comput Appl. 2018;30:3467–78.
[9] Das SK, Choi SUS, Yu W, Pradeep T. Nanofluids: science and technology. Hoboken, NJ, USA: John Wiley & Sons, Inc; 2008. p. 397.
[10] Ilyas SU, Pendyala R, Shuib AS, Marneni N. A review on the viscous and thermal transport properties of nanofluids. Adv Mater Res. 2014;917:18–27.
[11] Subramanian KV, Rao TN, Balakrishnan A. Nanofluids and their engineering applications. Florida, USA: CRC Press; 2020. p. 516.
[12] Boungiorno J. Convective transport in nanofluids. ASME J Heat Transf. 2006;128:240–50.
[13] Hojjat M, Etemad S, Bagheri R, Thibault J. Rheological characteristics of non-Newtonian nanofluids: Experimental investigation. Int Commun Heat Mass Transf. 2011;38:144–8.
[14] Ghanbarpour M, Haghigi EB, Khodabandeh R. Thermal properties and rheological behavior of water based Al_2O_3 nanofluid as a heat transfer fluid. Exp Therm Fluid Sci. 2014;53:227–35.
[15] Sica LUR, Contreras E, Bandarra Filho EP, Parise J. An experimental viscosity investigation on the use of non-Newtonian graphene heat transfer nanofluids at below-ambient temperatures. Int J Energy Res. 2021;45:14530–46.
[16] Rana P, Bhargava R, Anwar Bég O, Kadir A. Finite element analysis of viscoelastic nanofluid flow with energy dissipation and internal heat source/sink effects. Int J Appl Comput Math. 2017;3(2):1421–47.
[17] Vasu B, Kumar Ray A, Anwar Bég O, Reddy Gorla RS. Magneto-bioconvection flow of a Casson thin film with nanoparticles over an unsteady stretching sheet: HAM and GDQ computation. Int J Numer Methods Heat Fluid Flow. 2019;29(11):4277–309.
[18] Abbasi A, Farooq W, Riaz I. Stagnation point flow of Maxwell nanofluid containing gyrotactic micro-organism impinging obliquely on a convective surface. Heat Transf. 2020;49(5):2977–99.
[19] Khan MN, Nadeem S. MHD stagnation point flow of a Maxwell nanofluid over a shrinking sheet (multiple solution). Heat Transf. 2021;50(5):4729–43.
[20] Khan M, Malik MY, Salahuddin T, Khan F. Generalized diffusion effects on Maxwell nanofluid stagnation point flow over a stretchable sheet with slip conditions and chemical reaction. J Braz Soc Mech Sci Eng. 2019;41(3):1–9.
[21] Ahmed J, Khan M, Ahmad L. Stagnation point flow of Maxwell nanofluid over a permeable rotating disk with heat source/sink. J Mol Liq. 2019;287:110853.
[22] Ghasemian A, Dinarvand S, Adamian A, Sheremet MA. Unsteady general three-dimensional stagnation point flow of a Maxwell/Buongiorno non-Newtonian nanofluid. J Nanofluids. 2019;8(7):1544–59.
[23] Bai Y, Liu X, Zhang Y, Zhang M. Stagnation-point heat and mass transfer of MHD Maxwell nanofluids over a stretching surface in the presence of thermophoresis. J Mol Liq. 2016;224:1172–80.
[24] Jagwal MR, Ahmad I, Sajid M. Non-axisymmetric Homann stagnation point flow of Maxwell nanofluid towards fixed surface. Int J Mod Phys C (IJMPC). 2021;32(06):1–18.
[25] Ahmed A, Khan M, Ahmed J, Hafeez A, Iqbal Z. Unsteady stagnation point flow of maxwell nanofluid over stretching disk with joule heating. Arab J Sci Eng (Springer Sci Business Media BV). 2020;45(7).
[26] Irfan M, Khan M, Khan WA, Alghamdi M. Magnetohydrodynamic stagnation point flow of a Maxwell nanofluid with variable conductivity. Commun Theor Phys. 2019;71(12):1493.
[27] Acharya N, Das K, Kundu PK. Cattaneo-Christov intensity of magnetized upper-convected Maxwell nanofluid flow over an inclined stretching sheet: a generalised Fourier and Fick's perspective. Int J Mech Sci. 2017;130:167–73.
[28] Argoud A, Trouillet-Fonti L, Ceccia S, Sotta P. Morphologies in polyamide 6/high density polyethylene blends with high amounts of reactive compatibilizer. Eur Polym J. 2014;50(177–189):177–89.
[29] Bruce Brown S. Reactive compatibilization, Polymer blends handbook. New York: Wiley; 2014.

[30] Wang M, Yuan G, Han CC. Reaction process in polycarbonate/polyamide bilayer film and blend. Polymer. 2013;54(14):3612–9.
[31] Shukla N, Rana P, Anwar Bég O, Kadir A, Singh B. Unsteady electromagnetic radiative nanofluid stagnation-point flow from a stretching sheet with chemically reactive nanoparticles, Stefan blowing effect and entropy generation. Proc IMechE Part N-J Nanomater Nanoeng Nanosyst. 2018;232:69–82.
[32] Garvandha M, Narla VK, Tripathi D, Anwar Bég O. Modelling the impact of melting and nonlinear radiation on reactive Buongiorno nanofluid boundary layer flow from an inclined stretching cylinder with cross diffusion and curvature effects. In: Tripathi D, Shamra S, editors. Applications in nanotechnology, book chapter, energy systems and nanotechnology", "advances in sustainability science and technology" book series. Germany: Springer; 2021. p. 279–306.
[33] Adesanya SO, Falade JA, Jangili S, Anwar Bég O. Irreversibility analysis for reactive third-grade fluid flow and heat transfer with convective wall cooling. Alex Eng J. 2017;56:153–60.
[34] Shamshuddin MD, Mishra SR, Anwar Bég O, Kadir A. Unsteady reactive magnetic radiative micropolar flow, heat and mass transfer from an inclined plate with Joule heating: a model for magnetic polymer processing. Proc IMechE- Part C – Mech Eng Sci. 2019;223(4):1–8.
[35] Kamran M, Wiwatanapataphee B. Chemical reaction and Newtonian heating effects on steady convection flow of a micropolar fluid with second order slip at the boundary. Eur J Mechanics-B/Fluids. 2018;71:138–50.
[36] Khan MI, Alzahrani F, Hobiny A, Ali Z. Estimation of entropy generation in Carreau-Yasuda fluid flow using chemical reaction with activation energy. J Mater Res Technol. 2020;9:9951–64.
[37] Khan D, Khan A, Khan I, Ali F, ul Karim F, Tlili I. Effects of relative magnetic field, chemical reaction, heat generation and Newtonian heating on convection flow of Casson fluid over a moving vertical plate embedded in a porous medium. Sci Rep. 2019;9(1):1–18.
[38] Khan MI, Alzahrani F. Binary chemical reaction with activation energy in dissipative flow of non-Newtonian nanomaterial. J Theor Comput Chem. 2020;19:2040006.
[39] Irfan M, Khan M, Khan WA. Heat sink/source and chemical reaction in stagnation point flow of Maxwell nanofluid. Appl Phys A. 2020;126(11):1–8.
[40] Yang W-J, Mochizuki S, Nishiwaki N. Transport phenomena in manufacturing and materials processing. Amsterdam: Elsevier; 1994.
[41] Bergman TL, Viskanta R. Radiation heat transfer in manufacturing and materials processing. In: Menguc MP, editor. Radiative transfer-I. New York: Begell House; 1996. p. 13–39.
[42] Siegel R, Howell JR. Thermal Radiation Heat Transfer. New York, USA: MacGraw-Hill; 1972.
[43] Ramana Murthy JV, Srinivas J, Anwar Bég O. Entropy generation analysis of radiative heat transfer effects on channel flow of two immiscible couple stress fluids. J Braz Soc Mech Sci Eng. 2017;39:2191–202.
[44] Janardhana Reddy G, Kethireddy B, Anwar Bég O. Flow visualization using heat lines for unsteady radiative hydromagnetic micropolar convection from a vertical slender hollow cylinder. Int J Mech Sci. 2018;140:493–505.
[45] Uddin MJ, Anwar Bég O, Ismail AI. Radiative-convective nanofluid flow past a stretching/shrinking sheet with slip effects. AIAA J Thermophys Heat Transf. 2015;29(3):513–23.
[46] Hayat T, Qayyum S, Waqas M, Alsaedi A. Thermally radiative stagnation point flow of Maxwell nanofluid due to unsteady convectively heated stretched surface. J Mol Liq. 2016;224:801–10.
[47] Akinbo BJ, Olajuwon BI. Impact of radiation and chemical reaction on stagnation-point flow of Hydromagnetic Walters' B fluid with Newtonian heating. Int Commun Heat Mass Transf. 2021;121:105115.
[48] Mahanthesh B. Flow and heat transport of nanomaterial with quadratic radiative heat flux and aggregation kinematics of nanoparticles. Int Commun Heat Mass Transf. 2021;127:105521.
[49] Rana P, Mahanthesh B, Mackolil J, Al-Kouz W. Nanofluid flow past a vertical plate with nanoparticle aggregation kinematics, thermal slip and significant buoyancy force effects using modified Buongiorno model. Waves Random Complex Media. 2021;1–25. doi: 10.1080/17455030.2021.1977416.
[50] Rana P, Al-Kouz W, Mahanthesh B, Mackolil J. Heat transfer of TiO_2-EG nanoliquid with active and passive control of nanoparticles subject to nonlinear Boussinesq approximation. Int Commun Heat Mass Transf. 2021;126:105443.
[51] Sabu AS, Mackolil J, Mahanthesh B, Mathew A. Nanoparticle aggregation kinematics on the quadratic convective magnetohydrodynamic flow of nanomaterial past an inclined flat plate with sensitivity analysis. Proc Inst Mech Eng Part E: J Process Mech Eng. 2021;5:371. doi: 10.1177/09544089211056235.
[52] Swain K, Mahanthesh B. Thermal enhancement of radiating magneto-nanoliquid with nanoparticles aggregation and Joule heating: a three-dimensional flow. Arab J Sci Eng. 2021;46:5865–73.
[53] Liao S. Beyond Perturbation: Introduction to the Homotopy Analysis Method. Florida, USA: CRC Press; 2003.
[54] Zheng L, Liu N, Zhang X. Maxwell fluids unsteady mixed flow and radiation heat transfer over a stretching permeable plate with boundary slip and nonuniform heat source/sink. ASME J. Heat Transfer. 2013;135(3).
[55] Hayat T, Ullah I, Ahmad B, Alsaedi A. Radiative flow of Carreau liquid in presence of Newtonian heating and chemical reaction. Results Phys. 2017;7:715–22.
[56] Akinbo BJ, Olajuwon BI. Homotopy analysis investigation of heat and mass transfer flow past a vertical porous medium in the presence of heat source. Int J Heat Technol. 2019;37(3):899–908.
[57] Tripathi D, Anwar Bég O, Curiel-Sosa J. Homotopy semi-numerical simulation of peristaltic flow of generalized Oldroyd-B fluids with slip effects. Comput Methods Biomech Biomed Eng. 2014;17(4):433–42.
[58] Anwar Bég O, Rashidi MM, Bég TA, Asadi M. Homotopy analysis of transient magneto-bio-fluid dynamics of micropolar squeeze film: a model for magneto-bio-rheological lubrication. J Mech Med Biol (USA). 2012;12(3):1250051-1–21.
[59] Ramesh GK, Gireesha BJ, Hayat T, Alsaedi A. Stagnation point flow of Maxwell fluid towards a permeable surface in the presence of nanoparticles. Alex Eng J. 2016;55(2):857–65.

[60] Hayat T, Muhammad K, Farooq M, Alsaedi A. Melting heat transfer in stagnation point flow of carbon nanotubes towards variable thickness surface. AIP Adv. 2016;6(1):015214.
[61] Panigrahi L, Panda J, Swain K, Dash GC. Heat and mass transfer of MHD Casson nanofluid flow through a porous medium past a stretching sheet with Newtonian heating and chemical reaction. Karbala Int J Mod Sci. 2020;6(3):11.
[62] Mathew A, Areekara S, Sabu AS, Saleem S. Significance of multiple slip and nanoparticle shape on stagnation point flow of silver-blood nanofluid in the presence of induced magnetic field. Surf Interfaces. 2021;25:101267.
[63] Abel MS, Tawade JV, Nandeppanavar MM. MHD flow and heat transfer for the upper-convected Maxwell fluid over a stretching sheet. Meccanica. 2012;47(2):385–93.
[64] Megahed AM. Variable fluid properties and variable heat flux effects on the flow and heat transfer in a non-Newtonian Maxwell fluid over an unsteady stretching sheet with slip velocity. Chin Phys B. 2013;22(9):094701.
[65] Ujjini Bhojappa V, Zeb S. OHAM simulation of 3D transverse magnetic field in rotating flow of Maxwell nanofluid over a stretching sheet with chemical reaction and heat source/sink. Heat Transf. 2021;50(5):4152–70.